3D EFFECTS ON J–Q TRAJECTORIES FOR FRACTURE SPECIMENS AND APPLICATIONS TO CORRELATE FRACTURE BEHAVIOR

Luiz Augusto de Lima e Silva
Fracture Mechanics and Structural Integrity Group - *NVFRAC*
Graduate Student, Department of Naval Architecture and Ocean Engineering,
University of São Paulo, São Paulo, SP 05508–900, Brazil

Claudio Ruggieri
Fracture Mechanics and Structural Integrity Group - *NVFRAC*
Professor, Department of Naval Architecture and Ocean Engineering,
University of São Paulo, São Paulo, SP 05508–900, Brazil
E–mail: claudio.ruggieri@poli.usp.br

Abstract – *Extensive plastic deformation often precedes cleavage fracture in ferritic steels when tested in the ductile-to-brittle transition (DBT) region. The interaction of crack-tip plastic zones with nearby traction-free surfaces and with global plastic zones affects strongly the near-tip stresses which control the onset of cleavage fracture. The loss of a unique relantionship between the crack-tip stresses and J, most often termed as loss of crack-tip constraint, underlies the specimen geometry and loading mode effects on cleavage fracture toughness values. These effects remain an important technological issue in industrial applications of fracture mechanics and in on-going development of fracture testing standards and engineering critical assessment (ECA) procedures.This study describes the 3D effects of crack-tip constraint on macroscopic fracture toughness based upon the two-parameter J-Q methodology. Within this methodology, J sets the size scale over which large stresses develop while the second parameter (Q) scales the near-tip distribution. The paper addresses representative 3-D non-linear, finite element solutions which provide J-Q trajectories for common fracture specimens under bend and tensile loading. A central feature of the investigation is the adoption of a convenient 3D definition for parameter Q which enables correlation of fracture behavior for varying crack configurations.*

Keywords*: cleavage fracture, structural integrity, J-integral, Q-parameter, crack-tip constraint*

1. Introduction

Conventional fracture mechanics methodologies to assess unstable cracking behavior (cleavage fracture) of different cracked bodies (i.e., laboratory specimens and engineering structures) rely on the similarity of their respective crack tip stress and deformation fields. Under small scale yielding (SSY) conditions, a single parameter, such as the linear elastic stress intensity factor, K, and the J-integral (or, equivalently, the crack tip opening displacement, CTOD or δ), uniquely scales the elastic-plastic near-tip fields (see, e.g., the review by Hutchinson [1]). However, fracture testing of ferritic structural steels in the ductile-to-brittle (DBT) transition region consistently reveals a significant effect of specimen geometry and loading mode (bending *vs.* tension) in cleavage toughness values as measured by the critical parameters $K_{\rm Ic}$, J_c or δ_c, (see [2, 3] for illustrative data). These studies show significant elevations in the elastic-plastic fracture toughness for shallow crack SE(B) specimens and tension geometries of ferritic steels tested in the transition region, where transgranular cleavage triggers macroscopic fracture. At increased loads in a finite body, such as a cracked specimen or structural component, the initially strong SSY fields gradually change to fields under large scale yielding (LSY) as crack-tip plastic zones increasingly merge with the global bending plasticity on the nearby traction free boundaries. This phenomenon, often termed *loss of constraint*, contributes to the *apparent* increased toughness of shallow cracked and tension loaded geometries observed in fracture testing. Once SSY conditions no longer apply, larger J-values in the finite body are necessary to generate a highly stressed region ahead of crack tip sufficient to trigger cleavage. These features have enormous practical implications in defect assessment procedures, particularly repair decisions and life extension programs of in-service structures as well as structural design specifications.

The technological importance of fracture behavior for cracked structures under LSY conditions prompted the development of two-parameter fracture theories. Under fixed loading, such methodologies assume a separable form for the actual cracked-body fields in a high triaxiality fields (such as the SSY field) and a *constant* field which quantifies the level of crack tip stress triaxiality. These research efforts proceed along essentially two lines: (1) the J-T methodology building upon the elastic T-stress (see review by Parks [4]), and (2) the J-Q methodology developed by O'Dowd and Shih [5, 6] building upon the hydrostatic param-

eter Q. Both frameworks characterize families of self-similar fields which describe crack tip fracture states in the full range of high and low triaxiality: in each one, J sets the size scale over which large stresses and strain develop while the second parameter (T or Q) scales the near-tip distribution relative to the reference stress state. The addition of a second parameter (T or Q) leads to the construction of experimentally derived fracture toughness loci, rather than conventional, single-valued definitions of toughness. The *correlation* of fracture conditions across different crack geometries/loading modes of the same material (and temperature) then proceeds without recourse to detailed features of the crack tip separation processes. At identical values of the scalar parameters (J and Q or T), the crack tip strain-stress fields that drive the local fracture process have identical values as well.

The present study builds upon the J-Q approach using full 3-D solutions to characterize effects of constraint on fracture behavior for common fracture specimens. The analysis matrix considers conventional C(T), SE(B) and SE(T) fracture specimens with varying geometries (*i.e.*, different notch depth to specimen width ratio, a/W, as well as different loading point distance, H), and test conditions (pin-loaded ends *vs*. clamped ends). Under increased loading, each cracked configuration follows a characteristic J-Q trajectory which enables comparison of the corresponding crack-tip driving force curve. A key feature of this investigation is the adoption of a convenient 3-D definition for the hydrostatic Q-parameter which enables consideration of the coupling between in-plane and through-thickness effects on crack front fields (which are not captured in plane-strain analyses). While the analyses were conducted on relatively limited crack configurations, the results provide a strong support to use constraint-designed specimens in fracture assessments of low constraint structural defects.

2. The J-Q Theory

2.1. Two-Parameter Description of Elastic-Plastic Crack-Tip Fields

The characteristic feature emerging from a multi-parameter description of the (stationary) elastic-plastic crack tip fields in homogeneous materials is the use of a scalar parameter to quantify the magnitude of these fields. Here, the J-integral sets the size scale over which high stresses develop while the second parameter (the elastic T-stress or the hydrostatic Q-parameter) quantifies the level of stress triaxiality at distances of a few CTODS ahead of the crack tip. In particular, the J-Q characterization of mode I deformation for craked bodies proposed by O'Dowd and Shih (OS) [5,6] provides an *approximate* two-parameter description for the elastic-plastic crack tip fields based upon a triaxiality parameter more applicable under LSY conditions for materials with elastic-plastic response described by a power hardening law given by $\epsilon/\epsilon_0 \propto (\sigma/\sigma_0)^n$. Here, n denotes the strain hardening exponent, σ_0 and ϵ_0 are the reference (yield) stress and strain, respectively. Guided by detailed numerical analyses employing a modified boundary layer (MBL) model [7], OS identified a family of self-similar fields in the form

$$\sigma_{ij} = \sigma_0 \hat{f}_{ij}\left(\frac{r}{J/\sigma_0}, \theta, Q/\sigma_0\right), \tag{1}$$

where the dimensionless second parameter Q defines the amount by which σ_{ij} in fracture specimens differ from the reference SSY solution with $T = 0$.

Limiting attention to the forward sector ahead of the crack tip between the SSY model with the T-stress set to zero ($\mathrm{SSY}_{T=0}$) and the fracture specimen fields, OS showed that $Q\sigma_0$ corresponds effectively to a spatially uniform hydrostatic stress, i.e., the *difference* field relative to a high triaxiality reference stress state

$$\sigma_{ij} = (\sigma_{ij})_{\mathrm{SSY;T=0}} + Q\sigma_0\delta_{1i}\delta_{1j}\,; \quad |\theta| < \frac{\pi}{2},\ J/\sigma_0 < r < 5J/\sigma_0\ . \tag{2}$$

Operationally, Q is defined by

$$Q \equiv \frac{\sigma_{\theta\theta} - (\sigma_{\theta\theta})_{\mathrm{SSY;T=0}}}{\sigma_0}, \qquad \text{at } \theta = 0,\ r = 2J/\sigma_0 \tag{3}$$

where finite element analyses containing sufficient mesh refinement to resolve the fields at this length scale provide the finite body stresses. Here, we note that Q is evaluated at $r = 2J/\sigma_0$ for definiteness; however, OS and Cravero and Ruggieri [8] also showed that Q is virtually independent of distance in the range $J/\sigma_0 < r < 5J/\sigma_0$. Construction of a J-Q *trajectory* then follows by the evaluation of Eq. (3) at each stage in loading of the finite body. This procedure imposes no restrictions on models to describe material flow properties or incremental *vs*. deformation plasticity.

2.2. Extension of Q-Parameter to 3D Crack Configurations

For 3-D, Mode-I configurations, Shih et al. [9] argue that the near tip fields at locations sufficiently far from external surfaces approach the form of Eq. (NO TAG) as $r \to 0$. Thus, evaluation of difference fields by means

of Eq. (3) at each point s along a 3-D crack front, designated $Q(s)$, provides Q values using local J-values and stresses in planes perpendicular to the crack front; consequently, the opening mode crack-tip state is completely described by the pair $(J(s), Q(s))$ at each point along the crack front.

To facilitate correlations of fracture behavior in 3-D between fracture specimens and cracked pipelines (which follows the previous 2-D plane-strain analyses by Cravero and Ruggieri [8], an alternative definition for Q as suggested by Shih et al [9] is adopted in the present study. Building up the notion of an average value for J to characterize the average intensity of far field loading on the crack front, a convenient measure of average constraint for a segment of the crack front, $s_a \le s \le s_b$, is given by

$$Q_{avg} = \frac{1}{s_b - s_a} \int_{s_a}^{s_b} Q(s) ds \ , \qquad \text{at } \theta = 0,\ r = 2J/\sigma_0 \tag{4}$$

The above expression generalizes the overall constraint for 3-D cracked specimens and structural components by including the potentially strong variations of out-of-plane constraint near the stress-free surface, particularly for thin crack configurations.

3. Finite Element Procedures

3.1. Numerical Models for Fracture Specimens

Nonlinear finite element analyses are performed on full 3-D models for selected 1-T fracture specimens (with thickness $B = 25.4$ mm). The analysis matrix covers bend and tension loaded fracture specimens with varying geometry and crack sizes: C(T) with $a/W = 0.6$ ($H/W = 0.75$), SE(B) with $a/W = 0.1$, 0.5 ($S/W = 4$) and SE(T) with $a/W = 0.1$, 0.5 ($H/W = 6$). Here, a is the crack size, W is the specimen width and H is the distance between the pin loading or clamps. All fracture specimens have conventional geometry, *i.e.*, $W = 2B$. For the SE(T) specimens, the analyses are also expanded to consider the effect of loading conditions, pin-loaded ends *vs.* clamped ends; these specimens are denoted as SE(T)$_P$ and SE(T)$_C$. Figure 1 shows the geometry and specimen dimensions for the analyzed crack configurations.

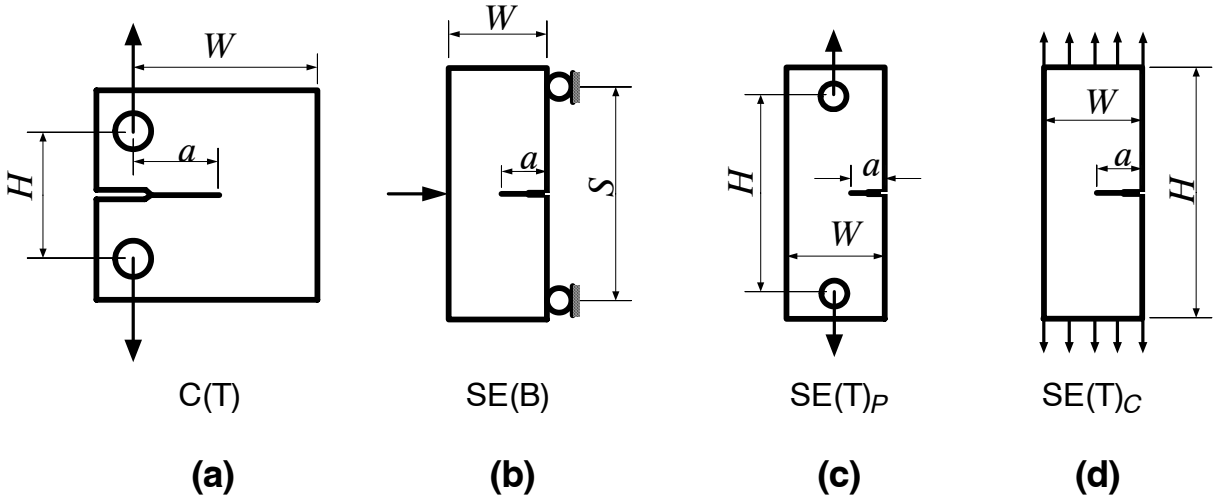

Figure 1 *Geometries for analyzed fracture specimens: (a) C(T) Specimen; (b) SE(B) Specimen; (c) Pin-loaded SE(T) Specimen and (d) Clamped SE(T) Specimen.*

Figure 2 shows the finite element model constructed for the 3-D analyses of C(T) specimen with $a/W = 0.6$. All other crack models have very similar features. A conventional mesh configuration having a focused ring of elements surrounding the crack front is used with a small key-hole at the crack tip; the radius of the key-hole, ϱ_0, is 2.5μm (0.0025 mm). Symmetry conditions enable analyses using one-quarter of the 3-D models with appropriate constraints imposed on the symmetry planes. The mesh has 15 variable thickness layers defined over the half-thickness ($B/2$); the thickest layer is defined at $Z = 0$ with thinner layers defined near the free surface ($Z = B/2$) to accommodate strong Z variations in the stress distribution. The quarter-symmetric, 3-D model for this specimen has 18030 nodes and 20800 elements. The finite element model is loaded by displacement increments to enhance numerical convergence.

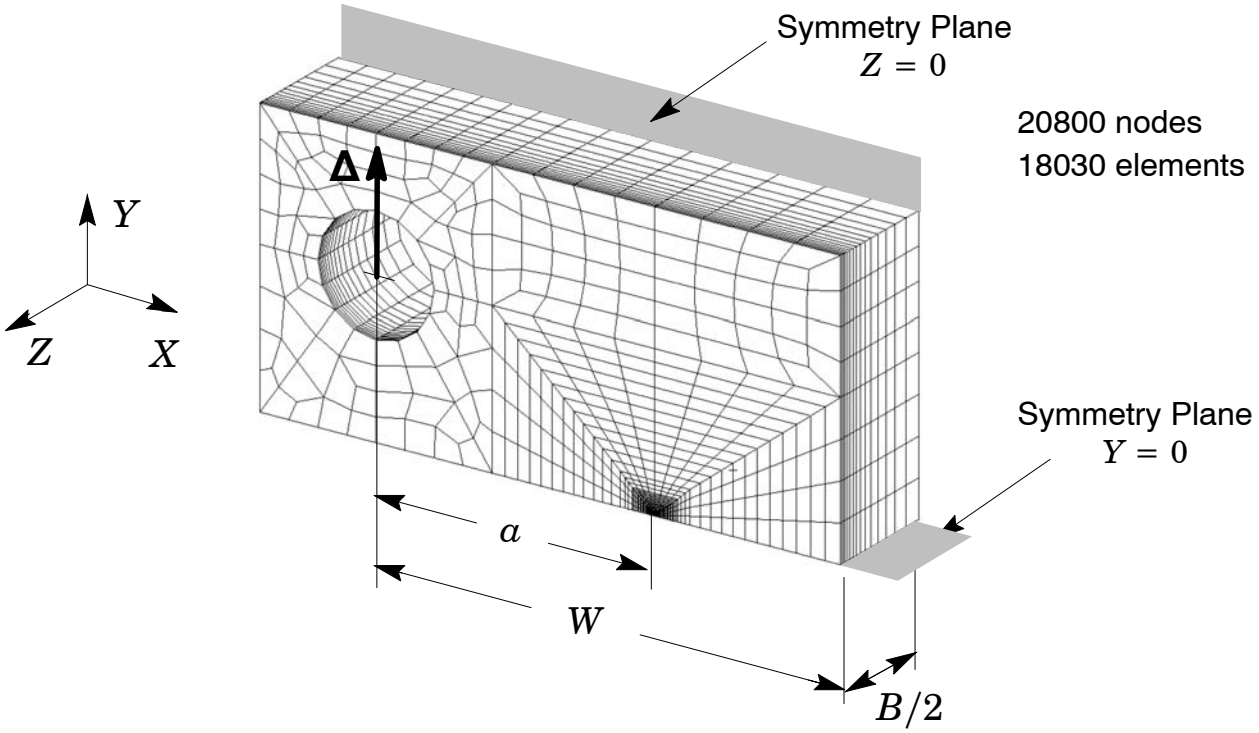

Figure 2 *Finite element 3-D model for the C(T) fracture specimen employed in the analyses.*

3.2. Numerical Solutions

The three-dimensional computations reported here are generated using the research code WARP3D [10] which: (1) implements a robust large strain formulation, nonlinear material response using the Mises constitutive model, (2) solves the equilibrium equations at each iteration using a very efficient, sparse matrix solver highly tuned for Unix and PC based architectures (3) evaluates the J-integral using a convenient domain integral procedure and (4) analyzes fracture models constructed with three-dimensional, 8-node trilinear hexahedral elements. Use of the so-called $\overline{\boldsymbol{B}}$ formulation [10] precludes mesh lock-ups that arise as the deformation progresses into fully plastic, incompressible modes. The sparse solver significantly reduces both memory and CPU time required for solution of the linearized equations compared to conventional direct solvers.

The elastic-plastic constitutive model employed in all analyses reported here follows a J_2 flow theory with conventional Mises plasticity in small geometry change (SGC) setting. The numerical solutions for the fracture specimens utilize a simple power-hardening model to characterize the uniaxial true stress-logarithmic strain in the form

$$\frac{\epsilon}{\epsilon_0} = \frac{\overline{\sigma}}{\sigma_0} \quad \epsilon \le \epsilon_0 \; ; \qquad \frac{\epsilon}{\epsilon_0} = \left(\frac{\overline{\sigma}}{\sigma_0}\right)^n \quad \epsilon > \epsilon_0 \tag{5}$$

where σ_0 and ϵ_0 are the reference (yield) stress and strain, and n is the strain hardening exponent. These finite element analyses consider a typical material flow property which is applicable to common pressure vessel steels: $n = 10$ ($E/\sigma_0 = 500$) with $E = 206$ GPa and $\nu = 0.3$.

4. 3-D Effects on J-Q Trajectories for Fracture Specimens

4.1. J-Q Trajectories Across the Crack Front for Deep Notch C(T) and SE(B) Specimens

To illustrate the strong interaction of in-plane and through-thickness effects on crack front fields (which are not captured in plane-strain analyses), this section provides J-Q trajectories at locations across the crack front derived from detailed 3-D analyses of conventinal fracture specimens. Figures 3 (a) and (b) show the J-Q trajectories generated under increased loading at locations $Z/(B/2)$ over the crack front for the 1-T

deep notch geometries with $n = 10$ (C(T) specimen with $a/W = 0.6$ and SE(B) specimen with $a/W = 0.5$). In these plots, Q is defined by Eq. (3) at the normalized distance ahead of crack tip given by $r = 2J/\sigma_0$ whereas J is normalized by $b\sigma_0$ with b denoting the remaining crack ligament $W-a$ (notice that we plot $J/b\sigma_0$ *vs.* $-Q$ to maintain positive scales). The research code JQCRACK [11] is employed to compute J-Q curves for each fracture specimen.

For the specimens in Fig. 3, Q-values are positive at low loads (corresponding to the positive elastic T-stress for this geometry [4]) except near the outside surface. Over the center portion of the specimen thickness, SSY conditions ($Q \geq 0$) exist strictly for low deformation levels. However, with increasing deformation, the hydrostatic parameter Q gradually changes to negative values which marks the loss of crack-tip constraint with increased levels of J. In contrast, near the outside surface, the specimens reveal large negative Q-values almost immediately upon loading which are associated with substantial reduction in the opening near–tip stresses for this specimen early in the loading. The differences between the constraint levels (as measured by Q) for the centerplane and along the crack front are specially prominent for points located at $Z/(B/2) \geq 0.5$.

To make contact with previous 2-D analyses conducted by Cravero and Ruggieri [8] and to facilitate comparisons with plane-strain conditions, Fig. 3 also includes plane-strain results for the analyzed configurations. Rather surprinsingly, the plane-strain analyses reveal that both specimens maintain higher levels of crack-tip constraint over the center portion. The difference between plane-strain and 3-D (centerplane) trajectories are essentially similar with continued loading. However, as already pointed out previously, the J-Q trajectories for points located outside the center portion of the specimen deviate significantly from the corresponding plane-strain trajectories.

4.2. J-Q Trajectories Across the Crack Front for SE(T) Specimens

Further insight into the effect of out-of-plane constraint can be gained by examining the J-Q trajectories at locations across the crack front for fracture specimens with similar geometry but subjected to different loading conditions. Figures 4(a-b) compare the effect of loading conditions (pin-load end *vs.* clamped ends) for the analyzed SE(T) specimens ($H/W = 6$); as introduce before, these specimens are denoted SE(T)$_P$ and SE(T)$_C$. Similarly to previous analyses, parameter Q is defined by Eq. (3) at $r = 2J/\sigma_0$ whereas J is normalized by $b\sigma_0$ with b denoting the remaining crack ligament $W-a$. Remarkably, the loading condition has a great effect on the J-Q trajectories along the crack front for the SE(T) specimens. The pin-loaded specimens display a rather strong dependence on $Z/(B/2)$. In contrast, the clamped specimens display a smaller dependence of J-Q trajectories on $Z/(B/2)$. Such differences in fracture behavior for the pin-loaded and clamped specimens (as described by their corresponding J-Q driving force curves in the present context) arise from the bending component in the loading history for the pin-loaded specimen.

5. Correlation of Fracture Behavior for Fracture Specimens in 3-D

The previous sections explore a constraint-based analysis for varying crack configurations based upon the J-Q methodology which clearly reveals the strong effects of in-plane and out-of-plane constraint on crack-tip fields. Such feature complicates interpretation of J-Q trajectories as an effective driving force which serves to characterize stress-controlled cleavage fracture in different crack configurations and subjected to varying loading conditions. To provide a more useful methodology to correlate fracture behavior in different cracked bodies, Fig. 5 presents the evolution of near-tip constraint with crack-tip loading (as measured by J) in terms of the generalized hydrostatic Q-parameter for 3-D cracks, Q_{avg}, as defined by Eq. (4).

Ths plots displayed in Fig. 5 show that the evolution of Q as loading progresses depends markedly on the specimen geometry. For the deep notch C(T) specimen with $a/W = 0.6$ and SE(B) specimen with $a/W = 0.5$, the Q-parameter is positive at low load levels (which corresponds to positive elastic T-stresses for these geometries [4]) and gradually change to negative (albeit small) values with increased levels of J. The pin-loaded , deep notch SE(T) specimen with $a/W = 0.5$ also displays a relatively similar behavior with comparable J-Q trajectories for almost the entire range of loading. In contrast, the clamped , deep notch SE(T) specimen with $a/W = 0.5$ displays much lower crack-tip constraint with increased J (as measured by larger negative Q-values). Further, all shallow crack geometries (SE(B) and SE(T) specimens with $a/W = 0.1$) reveal significant loss of crack-tip constraint almost immediately upon loading. Here, values for parameter Q ranging from -0.5 to -1.0 are associated with substantial reduction in the opening near–tip stresses for this specimen early in the loading.

6. Concluding Remarks

This study reports on full 3-D non-linear analyses of common fracture specimens which reveal strong effects of geometric parameters (a/W) and loading conditions on crack-tip constraint. To describe the evolving lev-

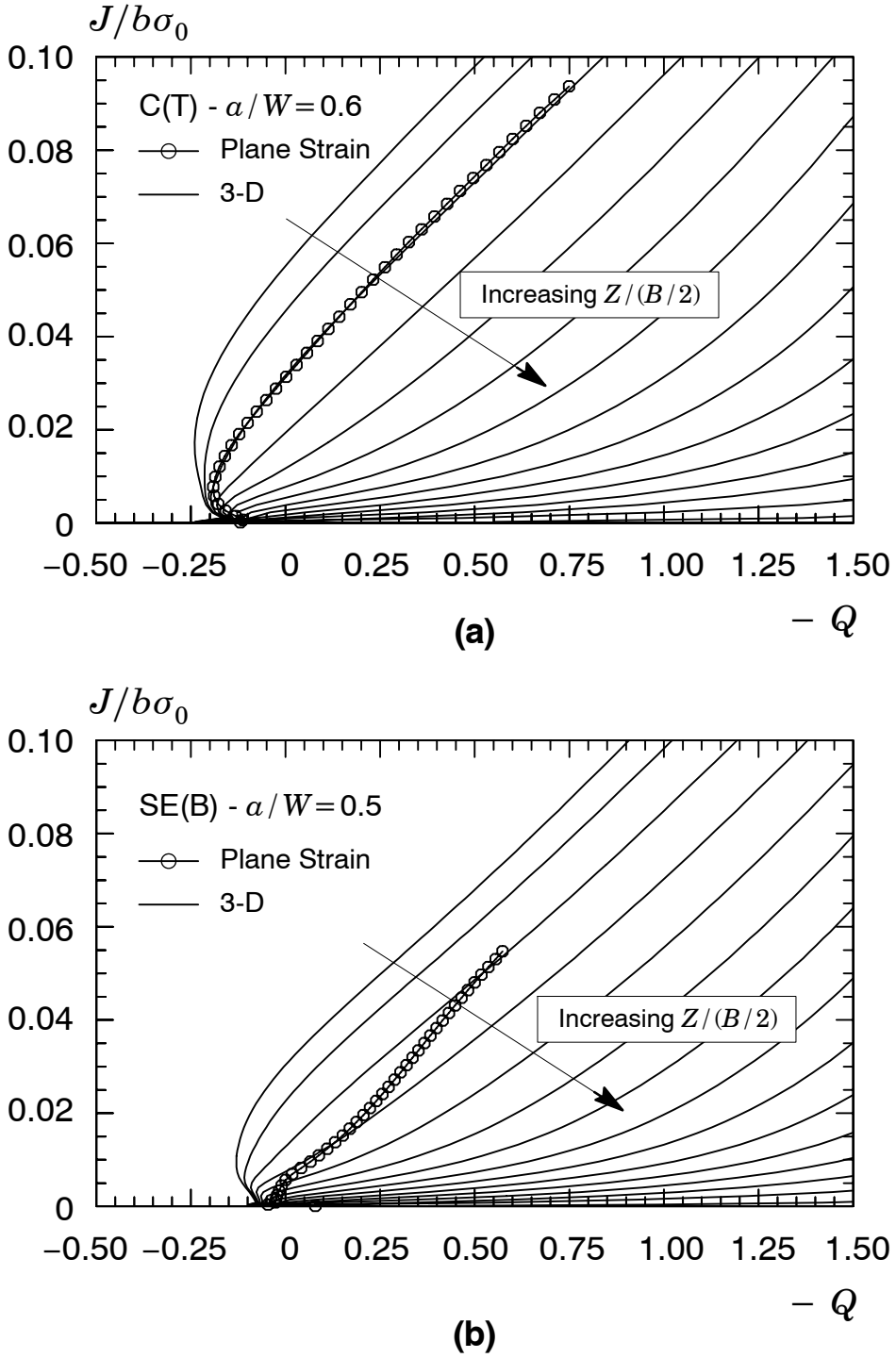

Figure 3 *J-Q trajectories across the crack front for deep notch fracture specimens with n = 10: (a) 1-T C(T) specimen with a/W = 0.6; (b) 1-T SE(B) specimen with a/W = 0.5.*

els of stress triaxiality ahead of crack front with increased loading, the present work employs the J-Q methodology to characterize stress-controlled cleavage fracture in different crack configurations and subjected to varying loading conditions. At similar values of the continuum, scalar parameters (J, Q), the crack-tip strain-stress fields which drive the local process have similar values as well. Consequently, cracked bodies with similar J-Q trajectories or driving force curves exhibit similar conditions for cleavage fracture. Such feature is central to proper choice of constraint designed test specimens in assessment procedures of cracked structural components. A key feature of this investigation is the adoption of a convenient 3-D definition for the hydrostatic Q-parameter, denoted Q_{avg}, which enables consideration of the coupling between in-plane and through-thickness effects on crack front fields (which are not captured in plane-strain analyses).

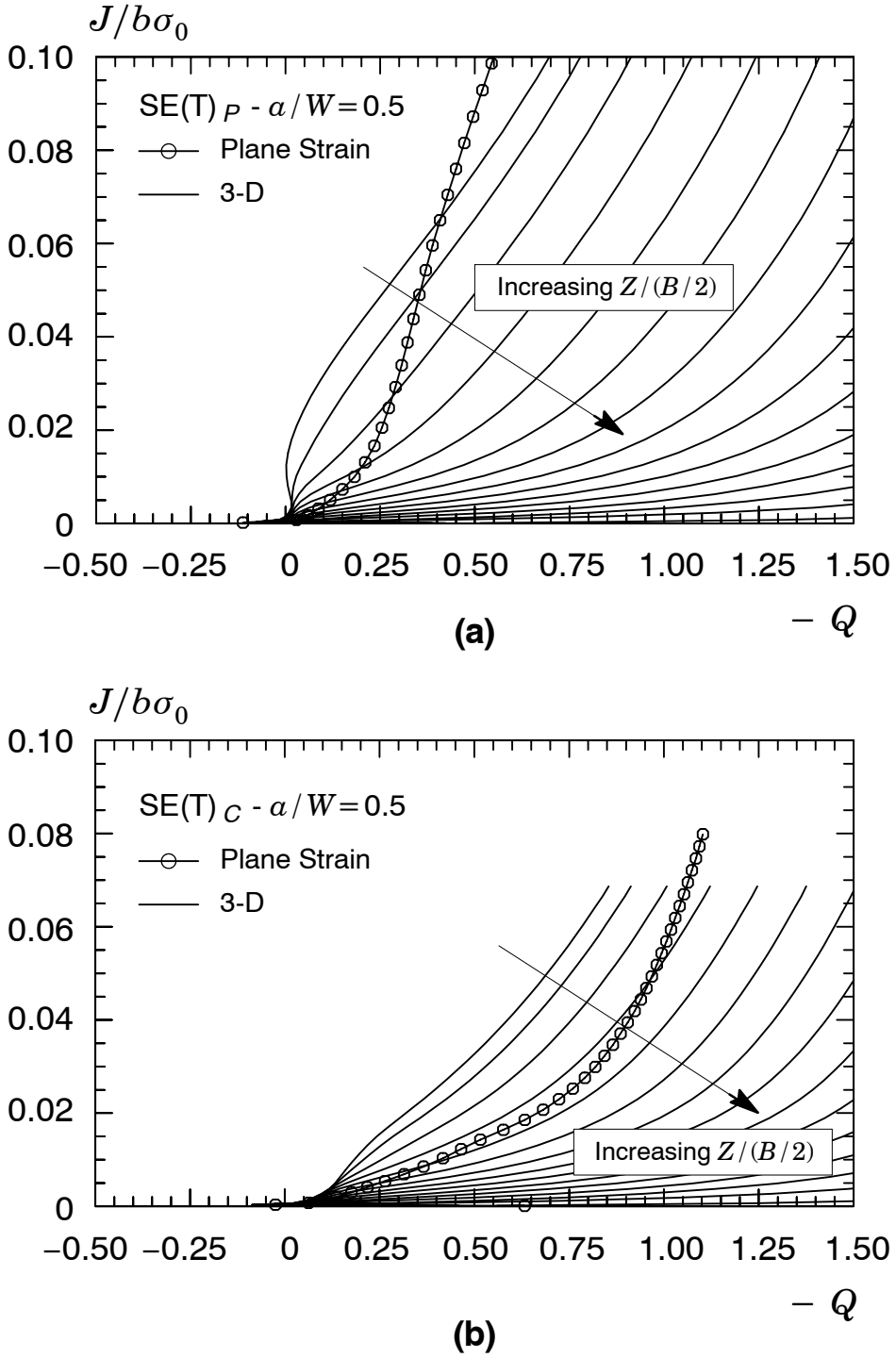

Figure 4 *J-Q trajectories across the crack front for deep notch SE(T) specimens with n = 10 and a/W = 0.5: (a) 1-T pin-loaded SET) specimen; (b) 1-T clamped SE(T) specimen.*

Construction of *J-Q* trajectories based upon the 3-D elastic-plastic crack-tip fields and Q_{avg} demonstrate the wide range of crack-tip constraint for varying specimen geometries, particularly for deeply cracked configurations. The present results, when taken together with previous studies of Cravero and Ruggieri, provide an additional body of results against which the applicability of constraint-designed fracture specimens in defect assessments of structural components can be weighed.

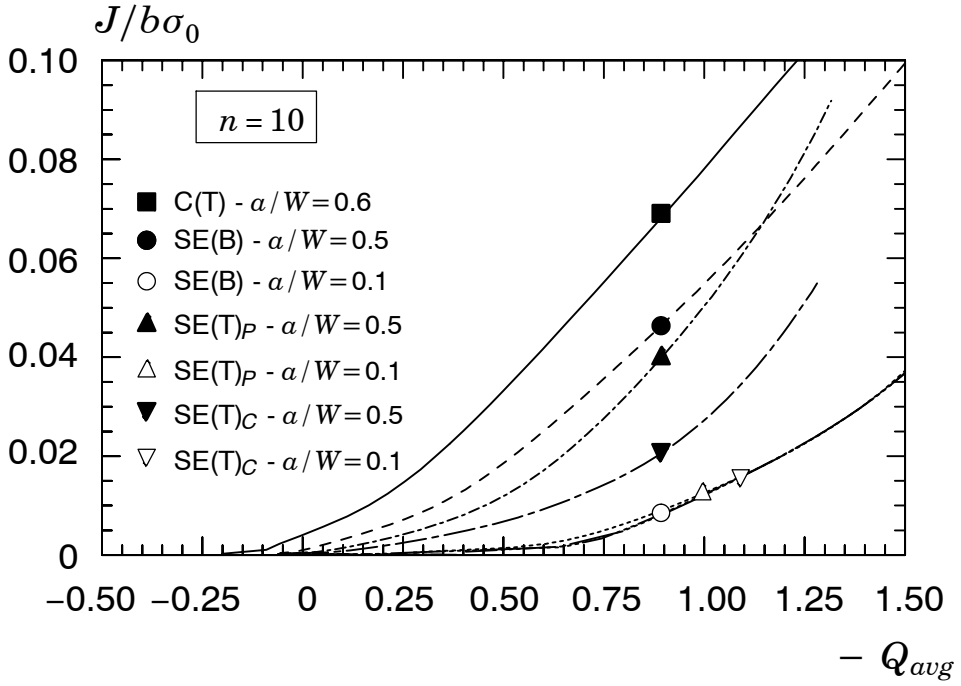

Figure 5 *J-Q trajectories for the analyzed fracture specimens with n = 10 based upon* Q_{avg}.

7. Acknowledgements

This investigation is supported by the State of São Paulo Research Foundation (FAPESP) through Grant 2003/02735-6. Funding to the second author (CR) is also provided by Conselho Nacional de Desenvolvimento Científico e Tecnológico (CNPq).

8. References

1. Hutchinson, J.W., "Fundamentals of the Phenomenological Theory of Nonlinear Fracture Mechanics," *Journal of Applied Mechanics*, Vol. 50, pp. 1042–1051, 1983.
2. Wiesner, C. S. and Goldthorpe, M. R., "The Effect of Temperature and Specimen Geometry on the Parameters of the Local Approach to Cleavage Fracture" in *International Conference on Local Approach to Fracture (MECAMAT 96)*, Fontainebleau, France, 1996, pp. C6-295–304.
3. Ruggieri, C. and Dodds, R. H., "A Transferability Model for Brittle Fracture Including Constraint and Ductile Tearing Effects: A Probabilistic Approach," *International Journal of Fracture*, Vol. 79, pp. 309-340, 1996.
4. Parks, D.M., "Advances in Characterization of Elastic–Plastic Crack–Tip Fields," in *Topics in Fracture and Fatigue,* A. S. Argon, Ed., Springer Verlag, pp. 59–98, 1992.
5. O'Dowd, N.P., and Shih, C.F., "Family of Crack–Tip Fields Characterized by a Triaxiality Parameter: Part I – Structure of Fields," *Journal of the Mechanics and Physics of Solids*, Vol. 39., No. 8, pp. 989–1015, 1991.
6. O'Dowd, N.P., and Shih, C.F., "Family of Crack–Tip Fields Characterized by a Triaxiality Parameter: Part II – Fracture Applications," *Journal of the Mechanics and Physics of Solids*, Vol. 40, pp. 939–963, 1992.
7. Larsson, S. G. and Carlsson, A. J., "Influence of Non–Singular Stress Terms and Specimen Geometry on Small Scale Yielding at Crack–Tips in Elastic–Plastic Materials", *Journal of the Mechanics and Physics of Solids*, Vol. 21, pp. 447–473, 1973.
8. S. Cravero and C. Ruggieri, "Assessments of Cleavage Fracture in High Pressure Pipelines with Axial Flaws Using Constraint Designed Test Specimens – Part I: Plane-Strain Analyses", *Engineering Fracture Mechanics*, Vol. 72, pp. 1344-1360, 2005.
9. Shih, C. F., O'Dowd, N. P. and Kirk, M. T., "A Framework for Quantifying Crack Tip Constraint" in *Constraint Effects in Fracture (ASTM STP 1171)*, pp. 2-20, 1993.
10. Koppenhoefer, K., Gullerud, A., Ruggieri, C., Dodds, R. and Healy, B., "WARP3D: Dynamic Nonlinear Analysis of Solids Using a Preconditioned Conjugate Gradient Software Architecture", *Structural Research Series (SRS) 596*, UILU-ENG-94-2017, University of Illinois at Urbana-Champaign, 1994.
11. Cravero, S. and Ruggieri, C. "JQCRACK - Numerical Computation of the Hydrostatic Parameter *Q* for 2D Cracked Structural Components", Technical Report BT-PNV-59, Politechnic School, University of Sao Paulo, 2003 (in Portuguese).

9. Responsibility Notice

The authors are the only responsible for the printed material included in this paper.